Drag Force and Clustering in Bubble Swarms

Ivo Roghair, Martin Van Sint Annaland, and Hans J. A. M. Kuipers
Multiphase Reactors Group, Dept. of Chemical Engineering and Chemistry, Eindhoven University of Technology, 5612 AZ Eindhoven, The Netherlands

DOI 10.1002/aic.13949
Published online November 15, 2012 in Wiley Online Library (wileyonlinelibrary.com).

In this article, results of detailed numerical simulations are reported meant to provide a closure relation for the drag force acting on bubbles rising in a dense swarm. The formation of clusters of bubbles in a periodic domain and the effect thereof on the rise velocity and effective drag coefficient on the bubbles are studied. Using smaller bubble sizes than presented in our earlier work, we are also able to refine our correlation for the drag coefficient acting on bubbles rising in a swarm, such that it is applicable for a large range of bubble sizes. The simulations are performed with an advanced Front-Tracking model in which Lagrangian marker points are used to track the gas–liquid interface, while accounting for surface tension and substantial interface deformation. Simulations were performed using periodic domains to simulate rising air bubbles in water from 1.0 mm up to 6.0 mm in diameter. The effect of liquid phase viscosity was also studied to extend the range of validity of the drag correlation. For the 1.0 and 1.5 mm cases, strong horizontal clustering effects are observed. Especially, at high gas fractions, the bubbles tend to form rigid horizontal arrays, which have been shown to strongly increase the drag force acting on the bubbles in the cluster. For viscous liquids, the tendency to form horizontal clusters is lower, and even vertical clustering is observed. The bubble slip velocity was compared with the experimental results of Zenit et al., which agree very well taking into account the differences between simulations and experiments. Based on our simulations, a new drag correlation was proposed, taking into account Eötvös numbers ranging from 0.13 to 4.9, and Morton numbers in the range $3.8 \leq \log Mo \quad 6.6$, and gas hold-ups up to 40% (30% for Eo 0.3). At lower values for log Mo, the Reynolds number drops to the order of unity, and the correlation overpredicts the drag coefficient, which defines the range of applicability of the currently proposed drag correlation. The correlation itself describes a linear increase of the normalized drag coefficient as a function of the gas hold-up. The strength of linear increase is stronger at lower Eötvös numbers. *AIChE J,* 59: 1791–1800, 2013
Keywords: bubble phenomena, fluid mechanics, multiphase flow, multiscale modeling

Introduction

Bubbly flows are often encountered in industrial processes that require the contact between a gas and a liquid. Examples from the chemical industry include phosgenation, oxidation, hydrogenation, and alkylation. Typically, these processes are performed in bubble columns, a liquid column in which a gas is injected at the bottom. The bubbles that form will rise, and (possibly reacting) components are exchanged between the bubbles and the liquid. Apart from the exchange of components, bubble columns can also be used for their mixing capabilities. For this reason, metallurgical applications use the injection of bubbles to achieve efficient mixing in molten steel. The wide-spread use of bubbly flows has lead to a considerable scientific interest since the 1970s, to enable optimization of process equipment.[1]

The gas hold-up (or gas fraction), denoted by α, is an important operational parameter to control the mass and heat transfer efficiency and hydrodynamics in a bubble column. At high gas fractions, bubbles form swarms that exhibit a behavior very different from single, undisturbed rising bubbles.

Multiscale modeling

Computational modeling provides an attractive tool to enhance or insight in complex multiphase flow processes. However, due to the large scale at which these processes operate, numerical simulations cannot be performed at full detail and full scale simultaneously. Therefore, we have adopted the multiscale modeling approach.[2] Using small scale, highly detailed direct numerical simulations (DNS), the forces acting on gas bubbles rising through a liquid can be described in a very accurate manner. These insights and correlations of these forces are used again in larger scale, but more coarsely resolved, models such as a discrete element method.[3]

The total force acting on a gas bubble rising through a liquid commonly contains contributions of the force of gravity $\overline{F}_G$, the liquid pressure gradient $\overline{F}_P$, drag $\overline{F}_D$, lift $\overline{F}_L$, and virtual mass $\overline{F}_{VM}$ (also termed added mass).

$$\overline{F}_{tot} = \overline{F}_G + \overline{F}_P + \overline{F}_D + \overline{F}_L + \overline{F}_{VM} \quad (1)$$

Using detailed simulations, dedicated experiments or analytical evaluation, the effect of these forces can be investigated.

Correspondence concerning this article should be addressed to I. Roghair at i.roghair@utwente.nl.

As a result, many correlations have been proposed, for instance, for the drag[4–6] and lift forces.[7–9] The majority of such correlations, however, are based on single, freely rising bubbles in an infinite quiescent liquid. The effect of swarms has gained more attention recently,[10–14] but many aspects of bubbles rising in swarms are still uncertain. An accurate description of the drag force experienced by bubbles rising in a swarm is crucial, because the residence time of bubbles in a bubble column reactor (and hence the efficiency of the process) is dominated by the drag force. It is, therefore, of major importance for large-scale numerical modeling, for instance, in application in Euler–Lagrange modeling techniques such as performed by Lau et al.[3]

Drag closure

In a recent work,[14] we have proposed a closure for the drag coefficient C_D acting on bubbles rising in a swarm. The derivation was based on DNS varying the Eötvös number ($Eo = \rho_c g d_b^2/\sigma$) between $1.2 \leq Eo \leq 4.8$ and varying the Morton number ($Mo = g\mu_c^4\Delta\rho/(\rho_c^2\sigma^3)$) in the range of $4 \times 10^{-12} \leq Mo \leq 2 \times 10^{-9}$ for gas fractions up to $\alpha = 0.45$

$$\frac{C_D}{C_{D,\infty}(1-\alpha)} = 1 + g(Eo)\alpha = 1 + \left(\frac{18}{Eo}\right)\alpha \qquad (2)$$

In this expression, the drag coefficient is normalized with the drag coefficient of a single rising bubble in an infinite liquid, $C_{D,\infty}$, and a correction factor for the gas hold-up $(1 - \alpha)$ is required, as a bubble rising in a dense swarm will experience a lower apparent density of the dispersed phase (see Roghair et al.[14] for a more elaborate explanation). The correlation shows a linear relation between the normalized drag coefficient and the gas hold-up, of which the slope is determined as a function $g(Eo)$ of the Eötvös number.

Grace[15] has published a detailed overview of the effect of the Morton, Eötvös, and Reynolds number ($Re = \rho_c v d_b/\mu_c$) on a single rising bubble. The diagram is shown in Figure 1, indicating the simulations of our previous work (red circles). It can be seen that the validity range of Eq. 2 is rather small, as the bubbles simulated are in the wobbling regime only.

With the additional simulations done for this work, it is possible to also extend the range of validity of the drag correlation. The Front-Tracking method is used to study different bubble sizes and liquid properties as indicated by the stars and bars in Figure 1. The Front-Tracking method used in this study neither allows bubbles to coalesce nor breaks up. This allows us to study the drag on a monodisperse swarm in a controlled fashion, because bubbles do not change size and the number of bubbles does not change. The model does, therefore, not handle bubbles with very large Eötvös numbers (spherical cap and skirted), because these bubbles do break up into multiple bubbles eventually.

Bubble clustering

Bubble clustering has been a popular research topic for decades. Horizontal clustering has been reported repeatedly, for pairs of clean, spherical rising bubbles,[16,17] and for bubbles rising in swarms.[18,19] In these works, generally spherical bubbles in the potential flow limit (i.e., small Weber number, large Reynolds number) are considered, yielding a preferred horizontal alignment due to Bernoulli effects. Bunner and Tryggvason[20] have provided a detailed outline of the microstructure of spherical and deformable bubbles using DNS at gas hold-ups up to 12%. It was reported that the vorticity

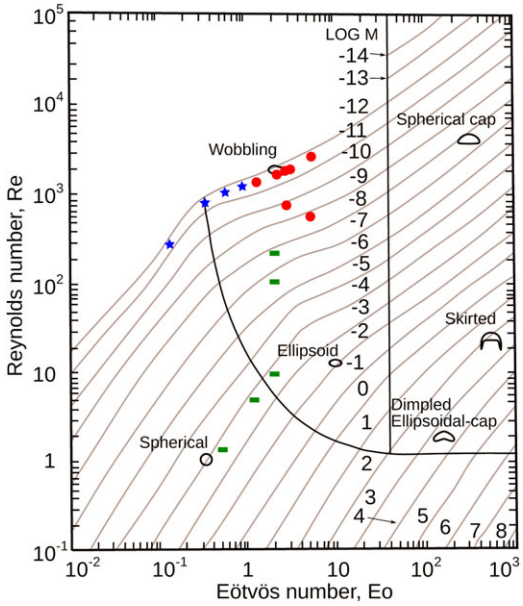

Figure 1. The diagram as presented in the work by Grace,[15] indicating the simulation data used for the drag correlation of Ref. 14 (red dots), and those of this work showing the extension to smaller bubble diameters for the air–water simulations with blue stars and bubbles in viscous liquids by the green bars.

[Color figure can be viewed in the online issue, which is available at wileyonlinelibrary.com.]

generated at the interface results in vertical attraction and horizontal repelling forces. This effect is stronger for larger bubbles, which, therefore, have a larger tendency to cluster vertically rather than horizontally. For spherical bubbles, the vorticity generated at the interface is much smaller, resulting in a smaller horizontal repelling force and thus allowing horizontal structures. The deviation from potential flow approximations is, therefore, larger for deformable bubbles. Measurements performed on the interstitial liquid velocities[21] have shown that the vorticity at low gas hold-ups (smaller than 2%) becomes important only at multiple bubble diameters away from the bubble, so locally potential flow can be assumed. At higher gas hold-ups, the wake interactions increase, and vorticity becomes more important near the bubble surfaces. The capability of DNS to cope with rotational flows is, therefore, important at higher gas fractions. In this work, we will further study the effect of horizontal clustering in periodic domains with our DNS code, at gas hold-ups up to 40%. In some cases, these clustering effects are found to be directly related to the periodic boundary conditions, having a strong effect on the drag experienced by the bubbles. These results will be described in detail but will be discarded from the drag closure analysis. In other cases, where clustering is not due to the periodic boundaries, the simulation results are integrally taken into account to determine the drag closure relation, and hence clustering effects are implicitly taken into account via the drag correlation.

Objectives

This work sets out to investigate the clustering effects of bubbles rising in a swarm at different gas hold-up and bubble diameters. Additionally, we use our simulation results to

Table 1. Numerical Settings Used for the Simulations Presented in This Work

Property	Symbol	Value
Mesh width	Δx	$\frac{d_b}{20}$
Domain size	n_x, n_y, n_z	Varies with α
Marker size (remeshing)		0.3–0.5 Δx
Time step	Δt	10^{-5} s
Simulation time	t_{end}	1.0–3.0 s

refine the correlation for describing the drag coefficient acting on rising bubbles in a swarm as proposed in Ref. 14 using a wider range of simulation parameters.

As air bubbles rising in water are a well-known base case, we will first extend the range of simulations of air–water to smaller bubble sizes, down to 1.0 mm, which can be compared with experimental results from the literature. A wide range of Morton numbers will be used by increasing the viscosity of the liquid phase to up to 50 times the viscosity of water.

This article continues with an outline of the Front-Tracking model, after which the simulation parameters will be described in detail. In the next section, we will continue to an analysis of bubble clustering effects, discussing the formation of horizontal planes in selected simulations. A comparison of the simulated bubble swarm rise velocity will be made to experimental results from the literature, followed by the refinement of the drag closure. We will wrap up with the main conclusions.

Front-Tracking Model

To solve the multiphase flows at the smallest scales, DNS are performed, which solve the fluid flow equations based on first principles, that is, the Navier–Stokes equations, without further assumptions. Because such simulations are typically computationally very expensive, a limited domain size must be chosen to keep simulation times within bounds. This work uses a Front-Tracking model, capable of simulating a swarm of rising bubbles using a periodic domain. The deformations of the bubble, relevant to any process taking place at the interface, are directly resolved by the model. Also clustering of the bubbles and its effect on the drag can be investigated in detail. A short introduction of the Front-Tracking method used for this work is given here. For a more detailed description, we refer to Dijkhuizen et al.[22]

The fluid flow is described with a single fluid formulation of the incompressible Navier–Stokes equation, whereas mass conservation is enforced by the continuity equation

$$\rho \frac{\partial \overline{u}}{\partial t} = -\nabla p - \rho \nabla \cdot (\overline{u}\overline{u}) + \nabla \cdot \overline{\overline{\tau}} + \rho \overline{g} + \overline{F_\sigma} \tag{3}$$

$$\nabla \cdot \overline{u} = 0 \tag{4}$$

where $\overline{u}$ is the fluid velocity, $\overline{\overline{\tau}}$ the stress tensor, and p the pressure. We use a finite difference technique to discretize the governing equations on a staggered grid. The solution of the governing equations is achieved using a two-step projection-correction method. The stress tensor is discretized semi-implicitly, and therefore, the three velocity components u_x, u_y, and u_z are solved separately (projection). Then, the mass balance is enforced via a pressure correction step. The resulting discretized equations are solved with an efficient incomplete Cholesky conjugate gradient (ICCG) method. The computational domain is bounded by full 3-D periodic walls, so that an infinite swarm of bubbles is mimicked.

The interface is tracked with homogeneously distributed Lagrangian marker points that build up a triangular mesh. In Eq. 3, $\overline{F}_\sigma$ accounts for the surface tension force, which can be directly calculated from the positions of these points.

After the fluid flow has been calculated, the Lagrangian marker points are moved to their new locations using an interpolated fluid velocity. We make use of cubic splines, which are constructed locally (i.e., in the vicinity of each bubble separately). The presence of other bubbles within this region does not affect the construction of the splines, because the flow field is continuous over the interface. The marker points are advected with the interpolated fluid flow using fourth-order Runge–Kutta time stepping. From the marker data, the centroid of the bubbles can be calculated and, hence, the position, velocity, and shape of the rising bubbles.

The phase fraction is derived from the marker position analytically; from the marker center positions, the volume of the bubble phase above each marker can be calculated for each Eulerian grid cell. The density of each Eulerian cell is calculated by weighted averaging with the phase fraction. The viscosity is obtained by harmonic averaging of the kinematic viscosities, also weighted by the phase fraction.[23]

Simulations

The extension of our simulation range toward smaller bubble diameters (i.e., $d_b = 1.0$ through $d_b = 2.5$ mm) compared to Ref. 14 has been indicated in Figure 1 using blue stars. Note that the Reynolds number depicted in the diagram is valid for single rising bubbles only. For all cases, we have verified that the Reynolds numbers resulting from the simulation of a single rising bubble in an infinite liquid corresponds to that indicated by Figure 1.

Simulations are performed using multiple bubbles in a periodic domain. The minimum number of bubbles required to accurately simulate a bubble swarm with all its features was determined to be 10 for wobbling bubbles[14] and 12 for spherical bubbles.[10] However, typically a number of 16 or 32 bubbles are simulated. The gas fraction is changed by altering the domain size, so that a small domain with 16 bubbles simulates a large gas hold-up, whereas the same 16 bubbles in a large domain mimic a low gas hold-up. We have used 20 grid cells in a bubble diameter. The default simulation parameters are those of air bubbles in water, of which the settings are given in Tables 1 and 2.

For the air–water regime, we have simulated bubbles with diameters d_b of 1.0–4.0 mm (with step 0.5 mm), and 6.0 mm. The used settings are given in Table 3, in which the Reynolds number is averaged over time and the total number of bubbles. The range indicates the Reynolds number for the lowest and highest used gas fraction.

Table 2. Physical Properties Set for the Air–Water Bubble Swarm Simulations

Property	Symbol	Value
Gas density	ρ_d	1.25 kg/m^3
Gas viscosity	μ_d	1.8×10^{-5} Pa s
Liquid density	ρ_c	1000 kg/m^3
Liquid viscosity	μ_c	10^{-3} Pa s
Surface tension coefficient	σ	0.073 N/m

Table 3. Bubble Diameters and Eötvös Numbers of the Air–Water Bubble Swarm Simulations

d_b (mm)	n_b	Eo	α	Re
1.0	16	0.134	0.05–0.40	147–34.4
1.5	16	0.302	0.03–0.40	336–78.3
2.0	16	0.537	0.05–0.40	429–200
2.5	16	0.839	0.05–0.40	573–271
3.0	16	1.21	0.03–0.42	735–330
3.5	16	1.64	0.03–0.42	851–422
4.0	32	2.15	0.05–0.45	910–513
6.0	32	4.83	0.05–0.45	1408–881

The Morton number for this gas–liquid system is $Mo = 2.5 \cdot 10^{-11}$.

Additionally, we have simulated bubbles in liquids with increased viscosity, leaving the other parameters constant. The Morton number was changed several orders of magnitude. Details are given in Table 4. These cases have been indicated in Figure 1 as green bars.

Results processing

We are especially interested in the time-averaged properties of the bubble swarm. Because the bubbles are initialized as stationary spheres, an initial transient period before the swarm reaches a statistical steady state has to be accounted for. Time averaging is required, because the bubble behavior is inherently dynamic due to the large amount of mutual interactions between the rising bubbles. Typically, the procedure involves the removal of the first 0.2 s of the simulation, which must be discarded before temporal and bubble-wise averaging can be performed. In some cases using lower gas fractions, small bubble sizes, and/or high viscosity liquids, this time interval is increased based on examination of the rise velocity profile over time.

Bubble Clustering in Periodic Domains

Bunner and Tryggvason[10,20] investigated the microstructure of the bubble swarm of spherical and deformable bubbles simulated using Front-Tracking simulations using an angular pair distribution function $G\ (r,\theta)$

$$G(r,\theta) = \frac{V}{n_b(n_b-1)} \left\langle \sum_{i=1}^{n_b} \sum_{j=1, i\neq j}^{n_b} \delta\left(\bar{r} - \bar{r}_{ij}\right) \right\rangle \qquad (5)$$

in which V is the volume of the periodic domain, $\bar{r}_{ij}$ is the vector between the two centroids of a pair of bubbles, and n_b is the number of bubbles. The angle θ is the angle between the vector connecting both centroids and the direction of gravity. Integrating $G(r,\ \theta)$ over the maximum radius r yields the angular pair distribution function $G\ (\theta)$ for an angular sector with width $\Delta\theta$ and radius r.

It was shown in Ref. 20 that the distribution function has a peak at $\theta = \frac{\pi}{2}$ for spherical bubbles, indicating horizontal clustering, which diminishes with increasing void fraction. In addition, increasing the separation distance r between two bubbles lowers the peak, indicating that the clustering is a local effect, and bubbles are nearly uniformly distributed over large distances.

We have performed angular pair correlations to characterize the distribution of the angle between pairs of bubbles. For the integration radius, r, we have chosen half the size of the periodic domain (i.e., $r = \frac{n_x d_x}{2}$), which is constant for a given α. The angular sector over which we integrate, $\Delta\theta$, was chosen to be $\Delta\theta = 5°$. From our experience with the analysis for these type of simulations, the time-averaging statistics were still sufficient in each angular section. The results are discussed in the following sections.

Table 4. Simulation Settings of the Swarm Simulations in Higher Viscosity Liquids

d_b (mm)	n_b	μ_c (Pa s)	$-\log Mo$	α	Re
2.0	16	5.0×10^{-02}	3.8	0.05–0.15	1.73–1.32
3.0	16	5.0×10^{-02}	3.8	0.05–0.15	5.11–4.12
4.0	16	5.0×10^{-02}	3.8	0.05–0.15	10.3–8.3
4.0	16	1.0×10^{-02}	6.6	0.05–0.15	82.1–67.1
4.0	16	5.0×10^{-03}	7.8	0.05–0.15	180–144

Air–water simulations

For a bubble volume concentration of 5%, the angular distribution function is given for the air–water simulations (Table 3) in Figure 2. The distributions show that horizontal clustering is observed strongly for the smallest bubbles (nearly spherical), but the peak decreases strongly with increasing bubble size. This agrees with the results by Bunner and Tryggvason.[20]

The strong tendency of near-spherical bubbles to cluster horizontally may cause undesired side-effects. For a specific domain size and number of bubbles, it is possible that the bubbles in the domain evolve to a stable horizontal aggregation state, leaving barely any space between the bubbles. When this happens, none of the bubbles will move out of such a structure. This can happen also if the bubbles form more than one plane. An example of such a case is given in Figure 3, depicting a snapshot of 16 bubbles of 1.0-mm diameter at a gas hold-up of 40%, where the bubbles are found in a structured packing in two planes.

Clearly this is an artifact of the domain size used. These aggregates will not break up, which differs from the behavior of bubbles rising in a swarm in an actual bubble column, where large-scale flow structures can provide a means to break up such clusters. We have discussed a way to calculate the maximum number of bubbles that can align

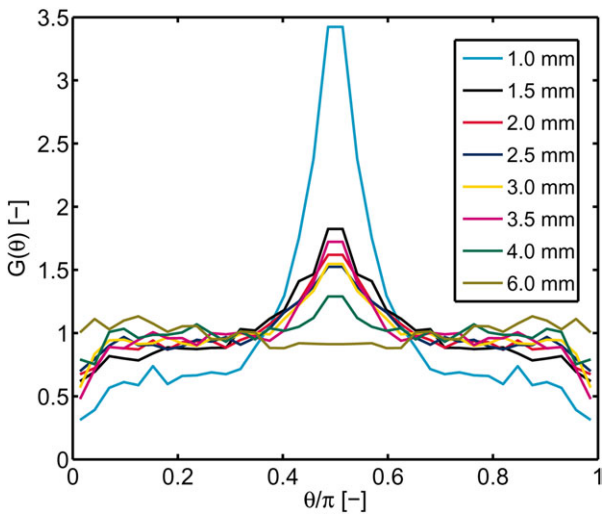

Figure 2. The angular pair distribution of air bubbles in water at a gas volume concentration of 5% and a radius $r/r_b = 5.5$.

[Color figure can be viewed in the online issue, which is available at wileyonlinelibrary.com.]

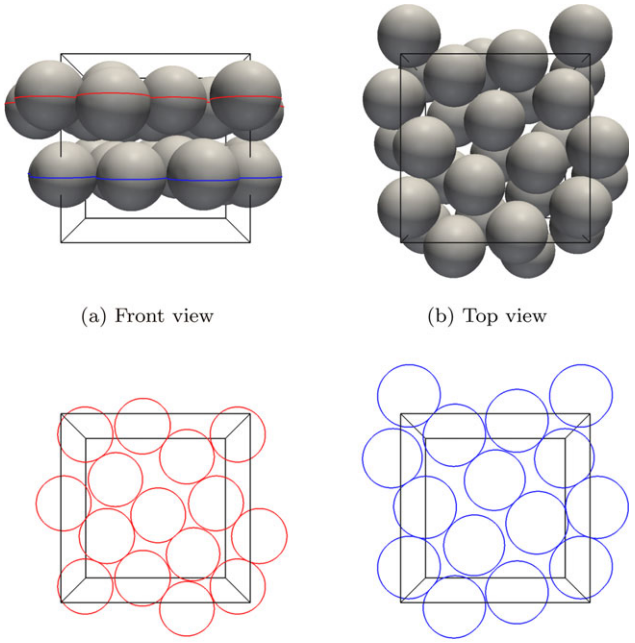

Figure 3. Horizontal cluster formation in a simulation using 16 × 1.0 mm air bubbles in water at a gas hold-up of 40% due to a balance between the number of bubbles and domain dimensions (domain size is 2.75 mm cubed).

This is Case 1 as presented in Table 5. The top images display the bubbles and the computational domain as seen from the front and top, whereas the bottom images display a slice of the bubble interface meshes at the center of each cluster plane. [Color figure can be viewed in the online issue, which is available at wileyonlinelibrary.com.]

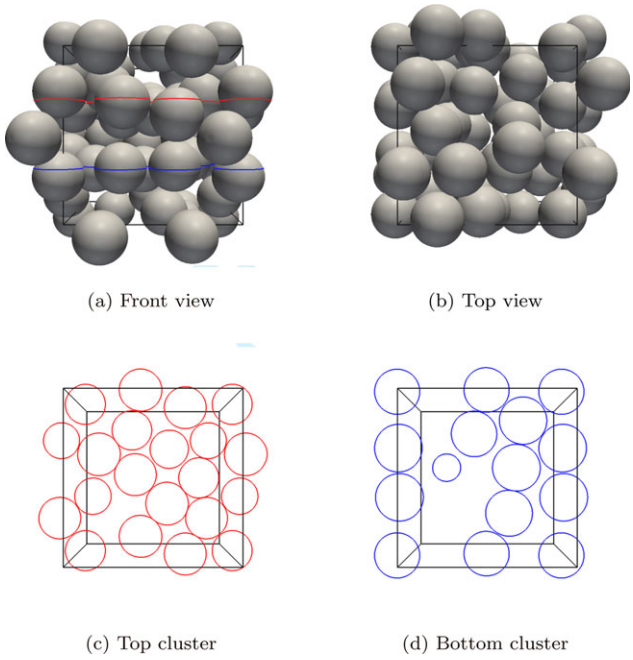

Figure 4. Same images as presented in Figure 3, now using a larger domain (3.45 mm cubed) and 31 bubbles to keep α constant at 40%.

This is Case 2 as presented in Table 5. The top images display the bubbles and the computational domain as seen from the front and top, whereas the bottom images display a slice of the bubble interface meshes at the center of each cluster plane (determined visually). While some horizontal clustering effects remain, they are much less pronounced than in the case presented in the previous figure.

in a horizontal plane $n_{b,max}$ as a function of the total number of bubbles n_b, the void fraction α, the bubble aspect ratio E, and the maximum horizontal packing fraction ϕ_{max}, assuming a cubic computational domain[24]

$$n_{b,max} = \frac{4\phi}{\pi}\left(\frac{n_b \pi E}{6\alpha}\right)^{\frac{2}{3}} \tag{6}$$

The bubble aspect ratio is given by

$$E = \frac{d_z}{\sqrt{d_x d_y}} \tag{7}$$

The packing fraction of randomly packed circles is about $\phi \approx 0.82$.[25] For the case depicted in Figure 3, $n_{b,max}$ can now be calculated to yield 7.9, which means that using 16 bubbles in this particular domain will yield $\frac{16}{7.9} \approx 2.03$ planes. If the ratio between n_b and $n_{b,max}$ is (close to) a whole number, and the aggregate is not disturbed by other factors such as heavily wobbling bubbles (large vorticity), the bubbles cluster together in $n_b/n_{b,max}$ horizontal aggregates that do not break up easily, and the results should be treated carefully.

Now consider an additional case with a larger number of bubbles ($n_b = 31$), but keeping the void fraction constant at $\alpha = 40\%$ (by increasing the domain size). Calculating the ratio $\frac{n_b}{n_{b,max}}$ now yields 2.51, indicating that two planes can be formed in close packing, but many bubbles are still able to move through the domain more freely. Although clustering in horizontal fashion still takes place, the stability of the formed structures is strongly decreased by the freely moving bubbles. Snapshots are shown in Figure 4, where we have aimed for creating a slice through the interfaces at the visually most dense location. It is clear that, although some horizontal alignment is still seen, larger liquid pockets between the bubbles are observed.

To illustrate the importance of the connection between the number of bubbles and the domain size once more, we have performed two simulations at a gas hold-up of $\alpha = 30\%$ (see Table 25). Similar to the cases discussed earlier, we find the bubbles distributed in two horizontal slabs in one case, where the ratio of n_b and $n_{b,max}$ is close to 2, and a more even distribution in the other case.

For the four cases mentioned in Table 5, we have performed an angular pair correlation analysis shown in Figure 5. It is observed that the tendency to horizontal clustering strongly decreases, if there are bubbles not confined in a

Table 5. Simulation Settings to Compare the Number of Bubbles Clustering in a Horizontal Plane

	$\alpha = 30\%$		$\alpha = 40\%$	
	Case 1	Case 2	Case 1	Case 2
n_b	16	24	16	31
$n_x = n_y = n_z$	61	69	55	69
$\frac{n_b}{n_{b,max}}$	1.66	1.95	2.03	2.51

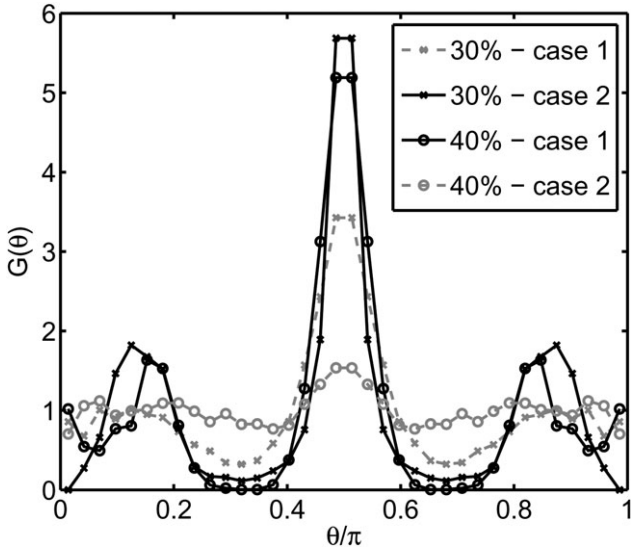

Figure 5. The angular pair distribution of the four cases given in Table 5, showing strong horizontal clustering for the cases where the number of bubbles fit exactly in a horizontal slab throughout the domain width.

slab. Additionally, for the cases where all the bubbles fill up a horizontal slab (30% Case 2 and 40% Case 1), a smaller peak indicating diagonal clustering is seen at about 20–30°, which is due to the alignment of the two slabs with respect to each other. For a face-centered cubic packing of spheres, the angle between two adjacent layers with the vertical axis is about 19°, whereas for a body-centered cubic packing a value of 30° is found. Conclusive evidence for the formation of these exact packing structures is omitted here, due to the lack of statistics with only tens of bubbles, which are still able to move within their slab a bit due to deformability of the particles and the transient nature of rising bubbles. It does, however, indicate that a simple cubic structure does not form here. The question remains whether such structures also emerge in real bubble columns, but experiments at such high gas fractions are very difficult to perform.

Due to these data, we choose to discard some of our spherical bubble cases (i.e., 1.0- and 1.5-mm diameter), where the $\frac{n_b}{n_{b,max}}$ yields a whole number, because we believe that the amplification of the clustering is due to a numerical artifact rather than the physics involved. However, we stress that much of the horizontal clustering we detect is genuine, that is, it is observed also in experimental[26] and other numerical works.[10]

The effect of such structure formations on the drag coefficient will be outlined in the drag section of this article.

Bubble swarms in viscous liquids

By increasing the viscosity as shown in Table 4, the Reynolds number decreases to the order of unity. Analyzing the angular distribution functions (with radius r over bubble radius r_b, $\frac{r}{r_b} = 2.75$) of these simulations (Figure 6), horizontal clustering is still found in most of these simulations, albeit not very pronounced. In fact, some simulations show signs of vertical clustering, especially, at the highest viscosities used. An indisputable clear trend misses here (for instance, the $\mu = 10\ \mu_w$ case does not show vertical clustering, in contrast to the $\mu = 5\ \mu_w$ and $\mu = 50\ \mu_w$). This may be due to the slowly rearranging bubbles (slow rise velocities), although the simulations of higher viscosity have ran for more than 4.0 s and based on visual inspection of the rise velocity profile, a statistically steady state has been reached. Due to the lower velocities and lack of shape deformations of the bubbles in viscous liquids, the interactions between bubbles are less strong (see also Ref. 20). This effect causes the bubbles to reorganize slower in the swarm. Therefore, not all angular sections were accounted for in large numbers to provide good statistics in all sections, despite the extended simulation period. It was found that this was improved using $\Delta\theta = 10°$ rather than 5° for the higher viscosity cases. Using these settings, a sufficient number of bins remain to discern the distribution for different values of θ.

We have compared the liquid velocity flow field for the 4.0-mm bubble swarm simulations with viscosities $\mu_c = 5 \times 10^{-3}$ Pa s and $\mu_c = 5 \times 10^{-2}$ Pa s (see Figure 7). The flow field of the less viscous case is clearly much more chaotic and bubbles are more deformed, whereas the streamlines of the viscous liquid are straight and smoothly curving around the bubbles. The viscous case shows much less horizontal pairing and a slight increase in vertical alignment. In

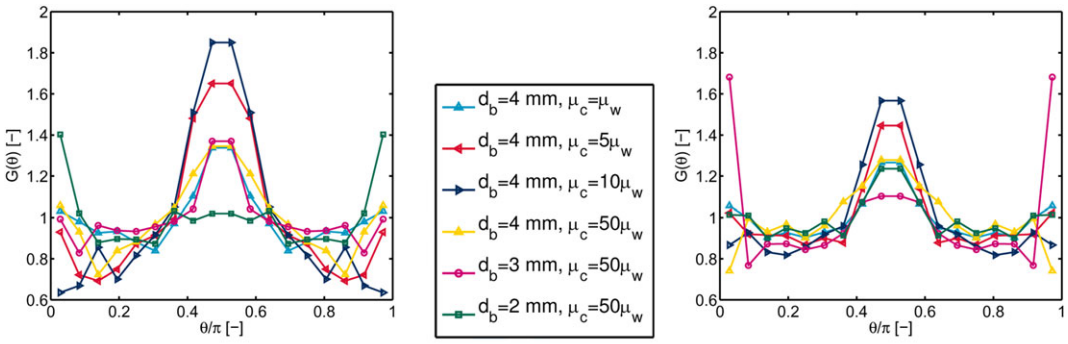

(a) $\alpha = 10\%$ (b) $\alpha = 15\%$

Figure 6. The angular distribution function of 10 and 15% gas hold-up simulations shows a tendency of vertical clustering.

The distribution function of 4.0-mm bubbles in water ($\mu_c = \mu_w$) and 5, 10, and 50 times more viscous liquids is depicted Additionally, the angular distribution function of 2.0- and 3.0-mm bubbles in $\mu_c = 50\mu_w$ is shown. [Color figure can be viewed in the online issue, which is available at wileyonlinelibrary.com.]

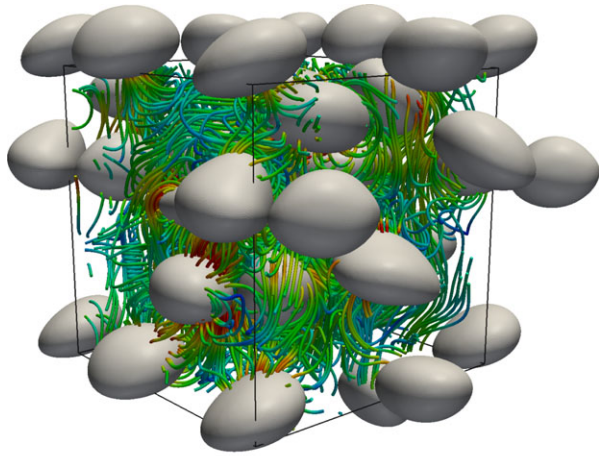

(a) $\mu_c = 5 \cdot 10^{-3}$ Pas

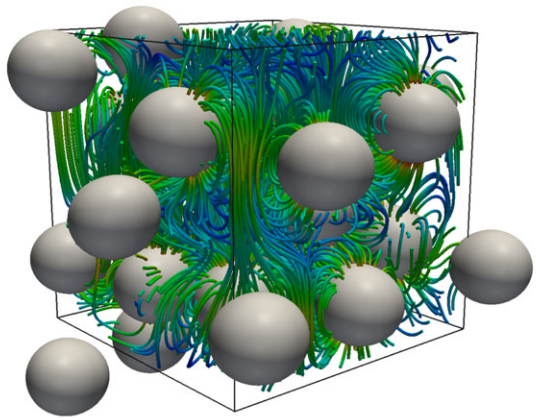

(b) $\mu_c = 5 \cdot 10^{-2}$ Pas

Figure 7. The liquid velocity flow field for two different liquid viscosities; the stream lines of the viscous case are much smoother and allow vertical clustering.

The colors on the streamlines indicate the velocity. In the viscous case, some channeling of the liquid between the bubbles can be seen due to an increase in vertical arrangement of the bubbles. In addition, the bubble shape is spherical in the viscous liquid, as opposed to the deformed bubbles (ellipsoidal/wobbling) in the inviscid case. [Color figure can be viewed in the online issue, which is available at wileyonlinelibrary.com.]

Figure 7b, the channeling of liquid between the bubbles can be seen; some of the vertical arrangements of the bubbles allow the liquid to flow from top to bottom not being influenced by the bubbles. This channeling effect can make part of the liquid pass through the swarm without encountering the bubble interfaces, hereby taking less or no part in, for instance, mass or heat transfer between the phases.

Bubble Rise Velocity

A comparison of our results will be made with the results from Zenit et al.,[27] who have performed measurements on monodisperse bubble swarms in vertical channel flow. Coalescence between bubbles was prevented using magnesium sulfate, which does not significantly influence the other physical parameters. They changed the gas hold-up by changing the gas flow through capillaries at the bottom of the column. A dual impedance probe was used to measure the bubble rise velocities. The bubble diameter deviates by about 10%, and the mean bubble diameter increases slightly with increasing gas hold-up from about 1.36 to 1.7 mm for α in the range between 0.0 and 0.2. A comparison will be made with data obtained from our simulations of monodisperse 1.5-mm bubbles with varying gas fractions between 0.05 and 0.4. We will use the vertical velocity component only in our analyses, which is justified by the horizontal velocity components being zero on average.

The results are shown in Figure 8. We have plotted the mean rise velocity of the bubbles through the domain, and the slip velocity, which is the bubble rise velocity relative to the mean liquid flow through the domain (which is pointed downward due to the upward motion of the bubbles and the periodic boundary conditions). The velocities obtained are lower than those measured by Ref. 27, up to a deviation of 25% in the range $\alpha \leq 0.20$. Curiously, the correlation proposed,[27] given as $v_b = v_{b,\infty} (1 - \alpha)^n$ with $v_{b,\infty} = 0.269$ for a single rising bubble, and $n = 2.796$ (dashed line in Figure 8), matches the slip velocity measured in our simulations in the range $0.2 \leq \alpha \leq 0.35$ within 10%.

The differences in the lower gas hold-up region can be explained by the lack of large-scale liquid velocity patterns in our simulations. In general, a vertical channel would display large-scale currents, induced by the bubbles. Although we can easily correct for the local liquid velocity by accounting for the average liquid velocity in the entire domain, it is very hard to obtain similar data simultaneously in experiments, especially, if large gas hold-ups are considered.

Other notable differences between simulations and experiments are the purity of the liquid, the much smaller domain size of the simulations (compared with typical experimental setups), and the (narrow) bubble size distribution we compare to. Moreover, in our simulations, we occasionally find bubbles going into the negative z direction (downward), due

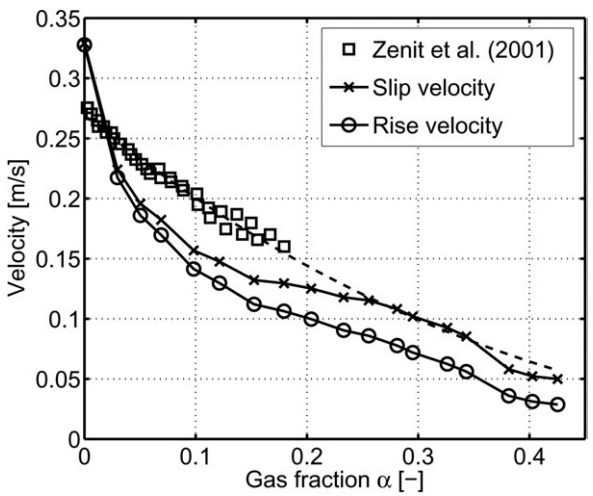

Figure 8. The averaged rise velocity and slip velocity of a swarm consisting of 16 × 1.5 mm air bubbles in water are compared with the experimental results extracted from Zenit et al.[27] and the correlation proposed (dashed line).

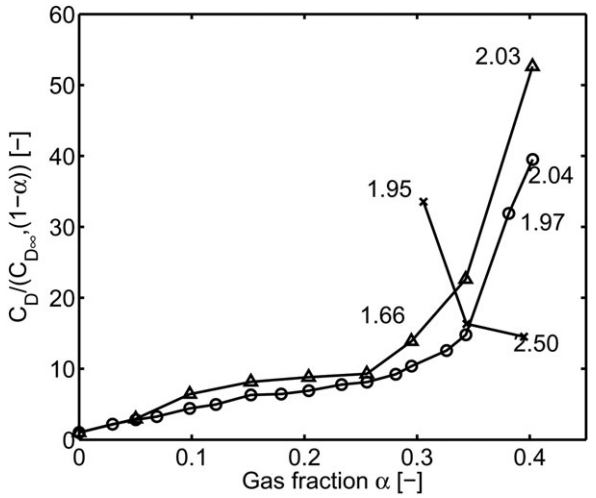

Figure 9. The normalized drag coefficient for 16 × 1.0 mm (△) and 16 × 1.5 mm (○) bubbles.

Additional simulation results for the 1.0 mm cases (×) with a different number of bubbles are also shown to show the influence of a coupled number of bubbles to the domain size. The numbers in the figure display the ratio $n_b/n_{b,max}$, which indicates the number of planes that can be formed by the bubbles in the domain.

to strong liquid velocity fluctuations. This effect decreases the average rise velocity from our simulations, but it is unclear how this phenomenon has affected the experimental results. Additional topics concerning the comparison between experiments and simulations in general were discussed in another work.[14]

In conclusion, we find a strong decrease of the bubble rise velocity, which is in itself in agreement with experimental observations,[27] as well as with dynamic potential flow simulations.[28]

The drop in velocity beyond $\alpha = 30\%$ is due to the formations of horizontal clusters, as explained in "Bubble Clustering in Periodic Domains" section. This issue will be further discussed in the next section.

Drag Force on Bubble Swarms

In this section, the influence of the observed clustering on the drag coefficient is investigated, followed by an adjustment of the drag correlation (Eq. 2) to a larger applicability range

Influence of clustering

We point out a tremendous increase in the drag of 1.0- and 1.5-mm bubbles beyond $\alpha = 0.30$. We have confirmed that stable horizontal clusters are of major influence on these results. We have plotted the 1.0 and 1.5-mm datasets and displayed the ratio $n_b/n_{b,max}$ alongside some of the data points in Figure 9.

We observed a strong correlation between clustering and an increase of the drag coefficient. Larger bubbles are less influenced by this effect due to the larger amount of vorticity they generate. Simulations with larger numbers of bubbles should give more insight in this phenomenon. At this time, such large simulations are not possible with our code due to the large computational demands. For the 1.0 and 1.5 mm cases, we will take into account gas fractions of $\alpha \leq 0.30$ only.

Air–water simulations

On basis of the selected subset of simulation results, we can still observe a linear increase of the normalized drag coefficient with increasing gas fraction (Figure 10a). The normalized drag coefficient of the smaller bubble sizes seems to bend upward beyond $\alpha \geq 0.4$, which we attribute to the lack of deformations in this regime due to spatial hindrance. Indeed, the bubbles have very little space to deform and remain more spherical. The simulations performed for

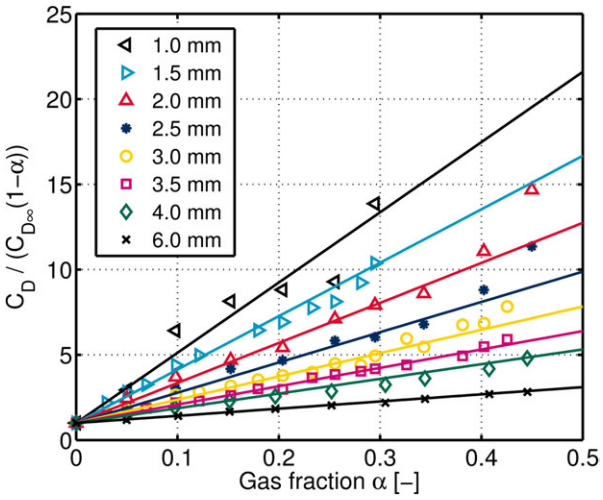

(a)

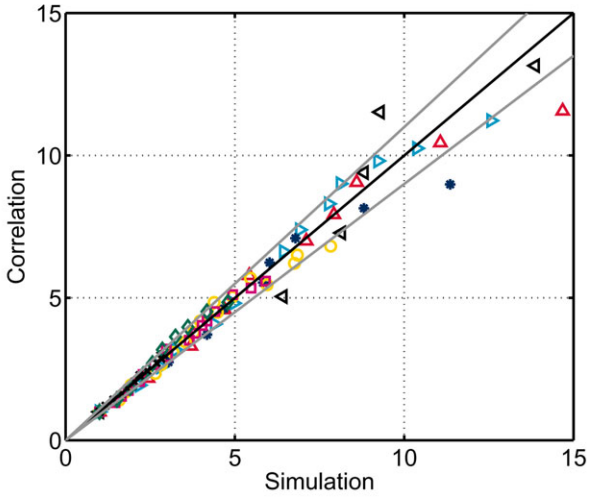

(b)

Figure 10. (a) The simulation results (combined with the results from Ref. 14) are plotted as marker points, together with the proposed drag correlation (lines) for different Eötvös numbers; (b) the normalized drag coefficient resulting from the new correlation is plotted vs. the simulation results in a parity plot to indicate results that deviate from the correlation.

The gray lines in the figure indicate a 10% deviation. In four cases, the simulations deviate more than 10% from the correlation, which mainly happens for smaller bubble sizes. [Color figure can be viewed in the online issue, which is available at wileyonlinelibrary.com.]

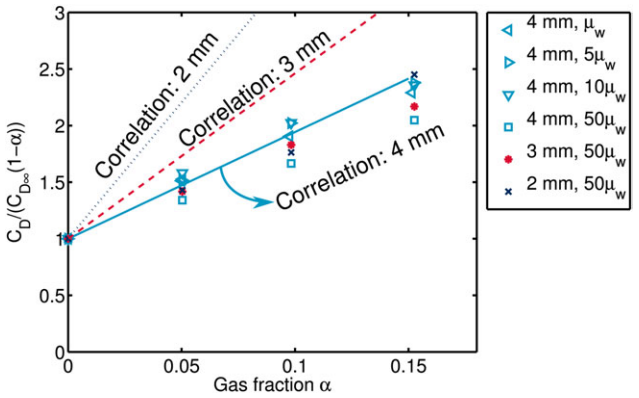

Figure 11. A comparison between the correlation and simulations with different viscosity.

The triangles show the 4.0 mm simulations at the viscosity of water ($\mu_c = \mu_w$), $5\mu_w$ and $10\mu_w$. These cases all agree with the proposed correlation (solid line). For the 4.0-mm bubbles in a liquid with $\mu_c = 50\mu_w$ (square), a lower result is obtained than predicted. The 2.0-mm (×) and 3.0-mm (*) bubbles in viscous liquid ($\mu_c = 50\mu_w$) also show a much lower drag than obtained with the correlation (dotted and dashed line, respectively). [Color figure can be viewed in the online issue, which is available at wileyonlinelibrary.com.]

this work do not supply enough data to provide an accurate fit for this effect, and a more detailed study into this effect can be undertaken in the future. Comparing our previous correlation to the current air–water simulations with smaller bubbles shows that Eq. 2 works fine for bubbles down to $d_b = 2.5$ mm ($Eo = 0.83$), but for smaller bubbles the drag coefficient is overestimated. The slopes of the individual data sets vary with the Eötvös number and were fitted using all datasets. These slopes were fitted to the Eötvös number to yield the closure correlation given in Eq. 8, yielding the lines displayed in Figure 10a.

$$\frac{C_D}{C_{D,\infty}(1-\alpha)} = 1 + \left(\frac{22}{Eo + 0.4}\right)\alpha \tag{8}$$

The parity plot shown in Figure 10b shows some individual cases where an individual simulation result differs over 10% from the correlation result. Especially, the lower Eötvös number bubbles deviate from the correlation. Larger bubbles deform easier and, therefore, move through the domain much more violently, whereas smaller bubbles may still occasionally get trapped in a stable situation, similar to the horizontal clustering effect. Although the simulated times are equal (over 1.5 s), the simulations with larger bubbles have better statistics. On average, our simulation results are described within 7% accuracy with Eq. 8.

The differences with the correlation proposed in Ref. 14 (Eq. 2) have been investigated. The normalized drag coefficient for Eötvös numbers below 1 is significantly lower (more than 10%) in the newly proposed correlation. This is expected, because this is the first time that lower Eötvös numbers have been taken into account. For Eötvös numbers larger than 2, the difference approaches 6% on average (averaged over a range of $0 \leq \alpha \leq 0.5$).

High-viscosity liquids

The normalized drag coefficient of bubbles rising in a swarm obtained from simulations with liquids with a high viscosity (Table 4) has been compared with the proposed drag correlation, Eq. 8. It was observed that for 4.0-mm bubbles rising in liquids with viscosities 5 times and 10 times larger than the viscosity of water ($-\log Mo = 7.8$ and 6.6), the correlation still perfectly fits the simulation results (see Figure 11). For the simulation cases of 2.0-, 3.0-, and 4.0-mm bubbles in a liquid with 50 times the viscosity of water ($-\log Mo = 3.8$, with Reynolds numbers in the order of unity), the normalized drag coefficient is overpredicted, especially for the 2.0 and 3.0 mm cases. The drafting effect (tendency of vertical clustering) seen in these cases may be of influence here. For Reynolds numbers smaller than 70, and liquids with $-\log Mo < 6.6$, the correlation does not hold and further investigations are required. Using a similar procedure as in the previous section, we have found a correlation describing these results (Eq. 9), but as the validity range is very small, a more detailed study on the transition from Eq. 8 to Eq. 9 should be performed.

$$\frac{C_D}{C_{D,\infty}(1-\alpha)} = 1 + \frac{(6.612Eo + 2.023)}{Eo}\alpha \tag{9}$$

Conclusions

We have presented results of simulations for dense bubbly flows using a Front-Tracking model. For air bubbles rising in water, it was observed that horizontal clustering occurs strongly for bubbles with a diameter of 1.0 and 1.5 mm. In specific cases, the bubbles merge together into a structured configuration of multiple horizontal slabs. This effect can be predicted using geometrical analysis of the domain size and the number of bubbles present in the simulation. Such structure formations have been shown to have a significant influence on the effective drag coefficient at higher gas fractions, and we have strong indications that this is caused by the combination of periodic boundary conditions and specific domain sizes and number of bubbles. It has also been shown that this artificial effect disappears when the number of bubbles and the domain size are altered, then showing only genuine clustering effects. For swarms rising in highly viscous liquids, horizontal clustering was still prevailing in most simulations, whereas vertical clustering was also observed.

For validation purposes, experimental data by Zenit et al.[27] has been compared with our simulation data of 16 1.5-mm air bubbles in water, which shows a very good agreement taking into consideration the differences between simulation and experiment.

The drag closure presented in Ref. 14 for bubbles rising in a swarm has been modified to be applicable to a wider range of Eötvös numbers and Morton numbers, by adding results of newly performed simulations with smaller bubbles to the fitting data. We have shown evidence that the normalized drag coefficient increases linearly with increasing gas fraction. Although the correlations can cope with a large range of liquid properties, liquids with a viscosity 50 times higher than that of water cannot be accurately be described with the currently proposed correlation. Although the normalized drag coefficient still increases linearly with the gas hold-up up to $\alpha = 0.15$, the drag for these cases is much lower than predicted, which may be due to the vertical clustering seen in some cases. We can, therefore, state that the range of validity of Eq. 8 extends to $0.13 \leq Eo \leq 4.83$ and $6.6 \leq -\log Mo \leq 10.6$. Future work should include a

thorough investigation of the transition regime in the Morton range of $3.8 \leq -\log Mo < 6.6$.

Acknowledgments

This work is part of the research programme of the Foundation for Research on Matter (FOM), which is financially supported by the Netherlands Organisation for Scientific Research (NWO) and the industrial partners of the IPP-FOM programme.

Notation

Roman symbols

C_D = drag coefficient
d_b = bubble diameter, m
d_x,d_y,d_z = mesh size in x,y,z direction
E = aspect ratio
$\overline{F}$ = force, N
g = gravity constant, m/s^2
$G(r, \theta)$ = angular distribution function
n_b = number of bubbles
n_x,n_y,n_z = number of cells in x,y,z direction
p = pressure, Pa
r = radius, m
t = time, s
$\overline{u}$ = fluid velocity, m/s
v = bubble velocity, m/s
V = domain volume, m^3

Greek letters

α = gas fraction
θ = angle, $^\circ$
μ = dynamic viscosity, Pa s
ρ = density, kg/m^3
σ = surface tension coefficient, N m
$\overline{\overline{\tau}}$ = stress tensor, Pa
ϕ = packing fraction

Abbreviations and subscripts

b = bubble
c = continuous phase
d = disperse phase
D = drag
Eo = Eötvös number, $\frac{\rho_c g d_b^2}{\sigma}$
G = gravity
L = lift
Mo = Morton number, $\frac{g\mu_c^4\Delta\rho}{(\rho_c^2\sigma^3)}$
P = pressure
Re = Reynolds number, $\frac{\rho_c v d_b}{\mu_c}$
VM = virtual mass
w = water
W = wall
We = Weber number, $\frac{\rho_c v^2 d_b}{\sigma}$
x,y,z = Cartesian directions
∞ = single rising bubble in an infinite quiescent liquid

Literature Cited

1. Deen NG, Mudde RF, Kuipers JAM, Zehner P, Kraume M. *Bubble columns*. In: *Ullmann's Encyclopedia of Industrial Chemistry*. Weinheim: Wiley-VCH Verlag GmbH & Co. KGaA, 2010.
2. Deen NG, Van Sint Annaland M, Kuipers JAM. Multi-scale modeling of dispersed gas-liquid two-phase flow. *Chem Eng Sci*. 2004; 59:1853–1861.
3. Lau YM, Roghair I, Deen NG, Van Sint Annaland M, Kuipers JAM. Numerical investigation of the drag closure for bubbles in bubble swarms. *Chem Eng Sci*. 2011;66:3309–3316.
4. Mei R, Lawrence CJ, Klausner JF. A note on the history force on a spherical bubble at finite Reynolds number. *Phys Fluids*. 1994;6:418–420.
5. Tomiyama A. *Struggle with computational bubble dynamics*. In: *3rd International Conference on Multiphase Flow*. Lyon, France, June 8–12, 1998.
6. Dijkhuizen W, Roghair I, Van Sint Annaland M, Kuipers JAM. DNS of gas bubbles behaviour using an improved 3D front tracking model-Drag force on isolated bubbles and comparison with experiments. *Chem Eng Sci*. 2010;65:1415–1426.
7. Legendre D, Magnaudet J. The lift force on a spherical bubble in a viscous linear shear flow. *J Fluid Mech*. 1998;368:81–126.
8. Tomiyama A, Tamai H, Zun I, Hosokawa S. Transverse migration of single bubbles in simple shear flows. 2002;57:1849–1858.
9. Dijkhuizen W, Van Sint Annaland M, Kuipers JAM. Numerical and experimental investigation of the lift force on single bubbles. *Chem Eng Sci*. *Chem Eng Sci*. 2010;65:1274–1287.
10. Bunner B, Tryggvason G. Dynamics of homogeneous bubbly flows part I. rise velocity and microstructure of the bubbles. *J Fluid Mech*. 2002;466:17–52.
11. Simonnet M, Gentric C, Olmos E, Midoux N. Experimental determination of the drag coefficient in a swarm of bubbles. *Chem Eng Sci*. 2007;62:858–866.
12. Smolianski A, Haario H, Luukka P. Numerical study of dynamics of single bubbles and bubble swarms. *Appl Math Model*. 2008;32:641–659.
13. Dijkhuizen W, Roghair I, Van Sint Annaland M, Kuipers JAM. *Numerical derivation of the drag force coefficient in bubble swarms using a front tracking model*. In: *6th International Conference on CFD in the Oil and Gas, Metallurgical and Process Industries*. 2008:CFD08–070.
14. Roghair I, Lau YM, Deen NG, Slagter HM, Baltussen MW, Van Sint Annaland M, Kuipers JAM. On the drag force of bubbles in bubble swarms at intermediate and high Reynolds numbers. *Chem Eng Sci*. 2011;66:3204–3211.
15. Grace JR. Shapes and velocities of bubbles rising in infinite liquids. *Trans Inst Chem Eng*. 1973;51:116–120.
16. Biesheuvel A, van Wijngaarden L. The motion of pairs of gas bubbles in a perfect liquid. *J Eng Math*. 1982;16:349–365.
17. van Wijngaarden L. The mean rise velocity of pairwaise-interacting bubbles in liquid. *J Fluid Mech*. 1993;251:55–78.
18. Smereka P. On the motion of bubbles in a periodic box. *J Fluid Mech*. 1993;254:79–112.
19. Sangani AS, Didwania AK. Dynamic simulations of flows of bubbly liquids at large Reynolds numbers. *J Fluid Mech*. 1993;250:307–337.
20. Bunner B, Tryggvason G. Effect of bubble deformation on the properties of bubbly flows. *J Fluid Mech*. 2003;495:77–118.
21. Roig V, de Tournemine L. Measurement of interstitial velocity of homogeneous bubbly flows at low to moderate void fraction. *J Fluid Mech*. 2007;572:87–110.
22. Dijkhuizen W, Roghair I, Van Sint Annaland M, Kuipers JAM. *Chem Eng Sci*. 2010;65:1427–1437.
23. Prosperetti A. *Navier–stokes numerical algorithms for free-surface flow computations: An overview*. In: Rein M, editor. *Drop Surface Interactions*. Vienna and New York: Springer-Verlag, 2002:237–258.
24. Roghair I, Van Sint Annaland M, Kuipers JAM. *Drag force on bubbles in bubble swarms*. In: *7th International Conference on CFD in the Oil & Gas, Metallurgical and Process Industries*, Melbourne, Australia, 2009.
25. Kausch HH, Fesko DG, Tschoegl NW. The random packing of circles in a plane. *J Colloid Interface Sci*. 1971;37:603–611.
26. Martínez Mercado J, Chehata Gómez D, Van Gils DPM, Sun C, Lohse D. On bubble clustering and energy spectra in pseudo-turbulence. *J Fluid Mech*. 2010;650:287–306.
27. Zenit R, Koch DL, Sangani AS. Measurements of the average properties of a suspension of bubbles rising in a vertical channel. *J Fluid Mech*. 2001;429:307–342.
28. Spelt PDM, Sangani AS. Properties and averaged equations for flows of bubbly liquids. *Appl Sci Res*. 1998;58:337–386.

Manuscript received Apr. 10, 2012, and revision received Sept. 6, 2012.